Chinese Chemical Letters 37 (2026) 111812

Contents lists available at ScienceDirect

Chinese Chemical Letters

journal homepage: www.elsevier.com/locate/cclet

Targeting disulfidptosis for ovarian cancer therapy induced by nanodrugs carrying 6-aminonicotinamide

Nannan Fan[a,1], Zhen Zhang[a,1], Huiyan Zu[a], Xinkui Liu[a], Bin Wang[b], Xiuming Miao[c], Chu Chu[a], Yunhong Zhang[a], Xiaoxiao Zhu[a], Ping Li[a,d,*], Xia Li[a,e,*]

[a] Innovative Institute of Chinese Medicine and Pharmacy, Key Laboratory of Traditional Chinese Medicine Classical Theory, Ministry of Education, Jinan Key Laboratory of Traditional Chinese Medicine Immuneregulation, Traditional Chinese Medicine Immuneregulation Engineering Research Center of Shandong Province, Shandong University of Traditional Chinese Medicine, Ji'nan 250014, China
[b] The Second Affiliated Hospital of Shandong University of Traditional Chinese Medicine, Ji'nan 250001, China
[c] Affiliated Hospital of Shandong University of Traditional Chinese Medicine, Ji'nan 250014, China
[d] College of Chemistry and Chemical Engineering, Northwest Normal University, Lanzhou 730070, China
[e] College of Traditional Chinese Medicine, Shandong University of Traditional Chinese Medicine, Ji'nan 250355, China

ARTICLE INFO

Article history:
Received 14 May 2025
Revised 5 September 2025
Accepted 8 September 2025
Available online 9 September 2025

Keywords:
Antitumor agents
Nanoparticles
6-Aminonicotinamide
Disulfidptosis
Ovarian cancer therapy

ABSTRACT

Ovarian cancer (OC) manifests the second deadliest gynecologic malignancy and shows severe conventional therapies-resistance, underscoring the urgent need for new therapeutic interventions. Disulfidptosis, caused in solute carrier family 7 member 11 (SLC7A11)-overexpressing ($SLC7A11^{high}$) cancer cells under glucose deficiency, has emerged as an appealing alternative approach. Herein we identified the significantly high expression of SLC7A11 in OC, and demonstrated that disulfidptosis induced by 6-aminonicotinamide (6-AN) effectively kill $SLC7A11^{high}$ OC cells. Hence, to enhance the therapeutic effect of 6-AN, we engineered a novel nanodrug, FA-L@AI, utilizing folic acid (FA)-modified liposome, and also illustrated the detailed therapeutic mechanism. Upon exposed to FA-L@AI, $SLC7A11^{high}$ OC cells endured internal nicotinamide adenine dinucleotide phosphate (NADPH) pools deleting, which leads to cystine accumulations. The elevated cystine levels resulted in disulfide bonds formation in actin cytoskeletal protein, ultimately triggering disulfidptosis. FA-L@AI nanoparticles exhibited an impactful suppression of tumor cells growth through 6-AN-induced disulfidptosis both *in vitro* and *in vivo*. Consistently, mRNA transcriptomic analysis further elucidated the underlying mechanism of disulfidptosis. Altogether, our work displays a unique strategy mediating disulfidptosis for OC specific therapy.

© 2026 Published by Elsevier B.V. on behalf of Chinese Chemical Society and Institute of Materia Medica, Chinese Academy of Medical Sciences.

Ovarian cancer (OC) is a prevalent disease with a high mortality up to 70%, which allows it to become the second leading cause of death among gynecological cancers worldwide [1,2]. Current treatment primarily involves surgery combined with chemotherapy using agents like cisplatin or paclitaxel. However, such approach only provides temporary symptoms relief, with a five-year survival rate of just 30%–40%, and often results in drug resistance [3,4]. Immunotherapy, known for its reduced side effects, shows limited effectiveness with patient response rate of only 8%–15% [5]. Therefore, development of precise and effective treatments for OC is desperately needed.

At present, targeting cell death-related pathways has proven to be an effective strategy for cancer therapy [6–13]. Solute carrier family 7 member 11 (SLC7A11) plays a pivotal role in facilitating cystine uptake and promoting glutathione synthesis. Under glucose-deprived condition, $SLC7A11^{high}$ cells experience a depletion of nicotinamide adenine dinucleotide phosphate (NADPH), which hinders cystine breakdown and leads to an accumulation of intracellular disulfides, inducing disulfide stress [14–16]. Subsequently, the abnormal disulfide bonds are formed in actin cytoskeletal protein, causing collapse of actin network [17,18]. The newly identified form of cell death, termed disulfidptosis, emerges a promising avenue for the precise treatment of $SLC7A11^{high}$ cancers [19–24]. Studies have already mentioned that SLC7A11 is over-expressed in OC patients [25]. Through bioinformatics analysis and Western blot (WB) analysis of clinical samples, we also revealed the high expression of SLC7A11 in OC tissues. Furthermore, our research shown enhancive levels of SLC7A11 in OC cells, where we observed an efficient induction of disulfidptosis under glucose-deprived condition. Therefore, targeting disulfidpto-

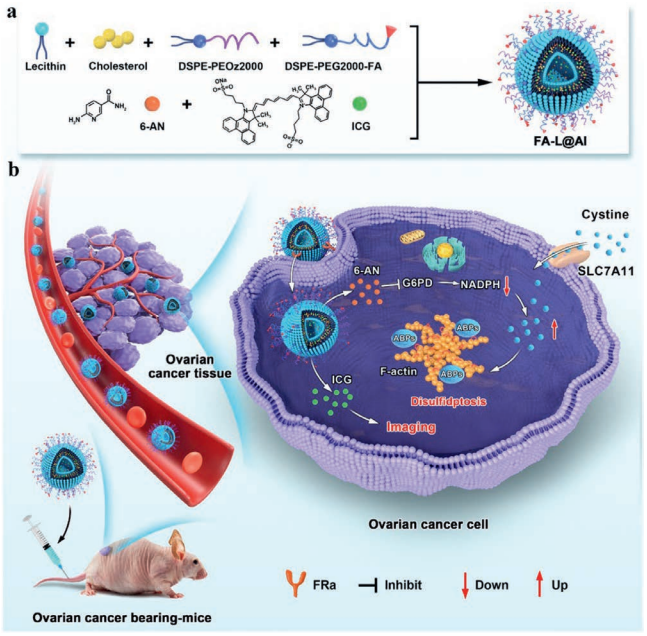
* Corresponding authors.
E-mail addresses: ip@sdnu.edu.cn (P. Li), 60230033@sdutcm.edu.cn (X. Li).
[1] These authors contributed equally to this work.

https://doi.org/10.1016/j.cclet.2025.111812
1001-8417/© 2026 Published by Elsevier B.V. on behalf of Chinese Chemical Society and Institute of Materia Medica, Chinese Academy of Medical Sciences.

sis in SLC7A11^{high} OC cells holds promise as a precise therapeutic strategy for OC.

Inhibiting NADPH, that is mainly synthesized by the pentose phosphate pathway (PPP), is critical for initiating disulfidptosis in SLC7A11^{high} cells. So, we focused on glucose-6-phosphate (G6P) dehydrogenase (G6PD), the rate-limiting enzyme of PPP. G6PD controls the entry of G6P into the PPP, thereby regulating NADPH level [26]. Researches have emphasized the negligible role of G6PD in OC, positioning it as a potential target [27]. 6-Aminonicotinamide (6-AN), a G6PD inhibitor, demonstrates robust capability of suppressing the PPP and blocking NADPH production in cells [28]. Based on this premise, we hypothesize that 6-AN could induce disulfidptosis in SLC7A11^{high} OC cells, offering a potential therapeutic approach for OC.

Due to the excellent biosafety and high drug-loading capacity, liposomes are widely utilized to establish nanosystems for drug delivery [29–34]. Employing photosensitizers or chemoradiotherapy drugs, extensive research efforts to exploit liposomal nanotherapeutics for OC treatment [35–40]. However, such methods frequently show unsatisfactory outcomes owing to suboptimal tumour specificity, phototoxicity side effect and complex synthesis process. Hence, we prepared a novel liposomal antitumor agents, FA-L@AI, which encapsulates 6-AN *via* a simple and rapid self-assembly synthesis. Simultaneously, the nanodrug leverages folic acid (FA) to enhance tumor uptake capability [41] and incorporates indocyanine green (ICG) as a fluorescent indicator [42–46] to assess the uptake and biodistribution of FA-L@AI (Scheme 1a). By design, the nanoparticles are preferentially trapped by OC cells attributed to the enhanced permeability and retention (EPR) effect [47,48] and the targeting ability of FA to folate receptor α (FRα), which mediates FA-L@AI may end up in lysosomes [49]. Owing to the acid-sensitive group PEOz2000, FA-L@AI cracks under acidic condition and releases drugs. Through 6-AN, this strategy is capable of inhibiting NADPH production, which leads to an increase in intracellular cystine levels, thereby occurring disulfidptosis in SLC7A11^{high} OC cells. ICG enables *in situ* imaging of cancer tissues (Scheme 1b). The nanodrug showed brilliant ability to restrain the growth of SLC7A11^{high} OC cells *via* disulfidptosis. In the animal study, FA-L@AI exhibited superior efficacy against OC growth compared to free 6-AN. In brief, FA-L@AI excellently achieves high efficient delivery of 6-AN, and establishes a new approach for specific treatment of OC.



Scheme 1. The fabrication of FA-L@AI and the proposed therapeutic mechanism, imaging of FA-L@AI for OC. (a) One-step synthesis of FA-L@AI through self-assembly, and the chemical structures of 6-AN, ICG, respectively. (b) *In vivo* initiation of intratumoral disulfidptosis and prediction of tumor growth inhibition using FA-L@AI.

To highlight the elevated expression of SLC7A11 in OC tissues, we initially analyzed the TCGA database, which revealed a remarkable overexpression of SLC7A11 in OC tissues (Fig. 1a). Furthermore, survival analysis found that SLC7A11^{high} OC patients showed considerably prolonged overall survival (OS) and progression-free survival (PFS) (Fig. 1b and Fig. S1a in Supporting information). Assessment of disulfidptosis-related genes suggested increased disulfidptosis activity in SLC7A11^{high} OC patients, correlating positively with SLC7A11 expression levels (Fig. 1c and Fig. S1b in Supporting information). Similar patterns were observed in the TCGA OC dataset (Figs. S1c–f in Supporting information). Importantly, we found that OC tissue was highly expressed the key gene SLC7A11 in clinical samples, indicating that disulfidptosis is a promising alternative approach for OC specific intervention (Figs. S2a–c in Supporting information). These results emphasized the elevated SLC7A11 expression in OC tissues, indicating a predisposition to occur disulfidptosis in OC.

To further confirm the correlation between SLC7A11 expression and disulfidptosis sensitivity, we selected OC cells OVCAR3, TOV-21G, A2780 and normal ovarian cells IOSE-29 to assess SLC7A11 protein levels. WB result showed that SLC7A11 was highly expressed in OVCAR3 and TOV-21G cells, whereas A2780 and IOSE-29 cells exhibited lower levels (Fig. 1d). We then evaluated whether SLC7A11 expression influences the sensitivity of OC cells to glucose deprivation-induced disulfidptosis. Cell counting kit-8 (CCK8) assays revealed that SLC7A11^{high} OC cells displayed a marked decrease in survival rate with prolonged glucose deprivation. In contrast, A2780 cells with low SLC7A11 expression, showed no substantial change in cell viability, suggesting that SLC7A11^{high} OC cells are particularly sensitive to glucose deprivation (Fig. S3a in Supporting information). Furthermore, glucose deprivation-induced cell death could be effectively mitigated by the thiol-specific reducing agent tris(2-carboxyethyl)phosphine (TCEP) [19], while other inhibitors such as ferroptosis inhibitor ferrostatin-1 (Fer-1), reactive oxygen species scavenger 1,2-dihydroxybenzene-3,5-disulphonic acid disodium salt monohydrate (Trion), apoptosis inhibitor Z-VAD(OH)-FMK (Z-VAD), and necroptosis inhibitor necrostatin-1 (Nec-1) did not rescue cell death under the same condition (Figs. S3b and c in Supporting information). More importantly, WB experiments demonstrated significant formation of disulfide bonds in actin cytoskeletal protein in SLC7A11^{high} cells under glucose deprivation (Figs. S3d and e in Supporting information). Collectively, these findings illustrated that glucose deprivation effectively induce disulfidptosis in SLC7A11^{high} OC cells, which predicts a potential therapeutic approach for OC.

Encouraged by the above results, we promptly sought drugs that could imitate the efficacy of glucose deprivation. TCGA data showed that the OS of SLC7A11^{high}/G6PD^{low} patient group was considerably longer than patient with SLC7A11^{low}/G6PD^{high} group in HGSOC, implying that inhibiting G6PD may be a viable therapeutic strategy for SLC7A11^{high} OC (Fig. 1e). Hence, we focused on the G6PD inhibitor 6-AN and investigated its potential to trigger disulfidptosis in SLC7A11^{high} OC cells. CCK8 assay uncovered a remarkable reduction in the survival rate of OVCAR3 and TOV-21G cells with increasing concentrations of 6-AN, whereas the viability of A2780 cells only decreased to 60%, indicating that 6-AN-induced cell death is dependent on SLC7A11 expression in OC cells (Fig. 1f). Similar to glucose deprivation, cell death caused by 6-AN could be effectively rescued by TCEP, but not by Fer-1, Trion, Z-VAD and Nec-1 (Figs. 1g and h). This suggested that 6-AN triggered the accumulation of disulfides. Given that preventing the reduction of

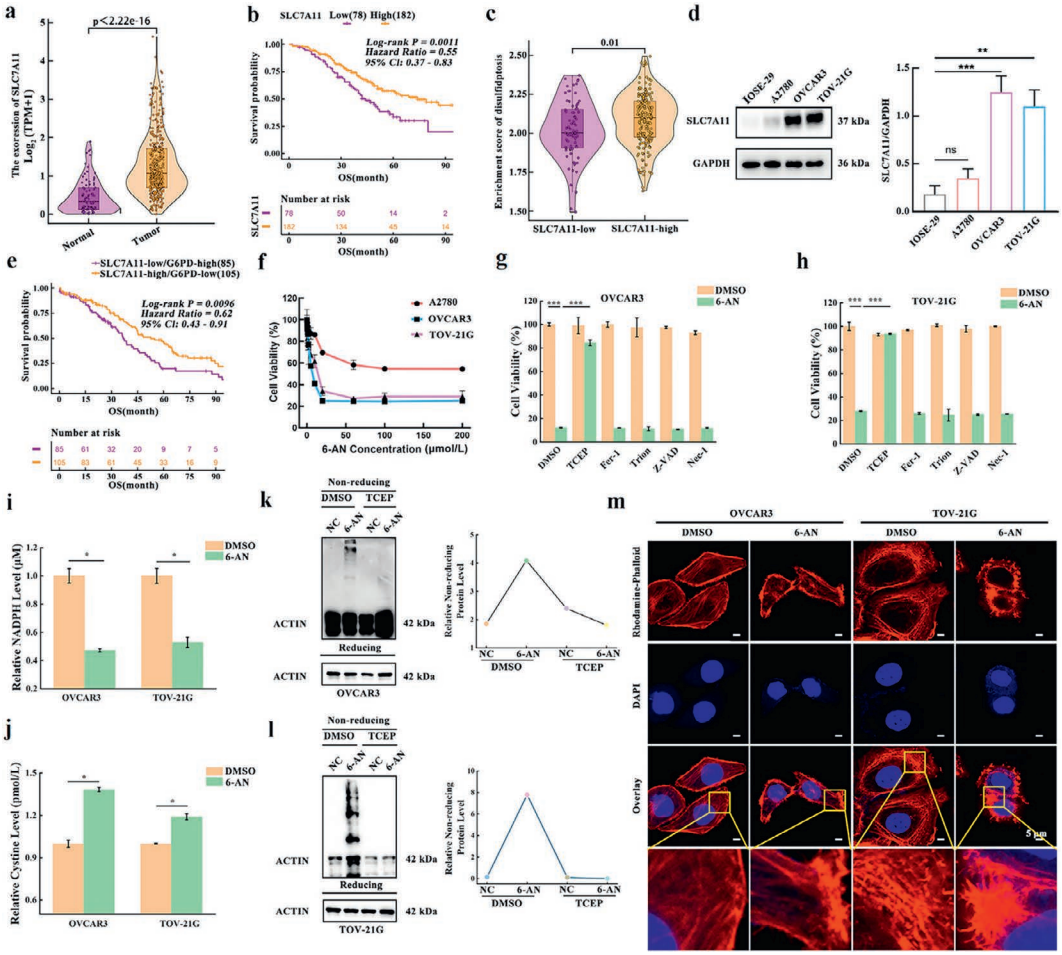


Fig. 1. 6-AN induces disulfidptosis in SLC7A11^{high} OC cells. (a) Differential expression of SLC7A11 between high-grade serous OC (HGSOC) tissues and normal tissues (based on TCGA-GTEx data). (b) Correlation between SLC7A11 expression and OS in HGSOC patients (based on GSE32062 data). (c) Comparison of enrichment scores for disulfidptosis between the SLC7A11^{high} and SLC7A11^{low} groups in HGSOC patients (based on GSE32062 data). (d) The expression of SLC7A11 in OC and normal cells. GAPDH, glyceraldehyde-3-phosphate dehydrogenase. (e) Correlation between SLC7A11, G6PD expressions and OS in HGSOC patients (based on TCGA data). (f) The dependence of SLC7A11^{high} OC cells on 6-AN. (g, h) Suppressing 6-AN-induced cells death by TCEP. (i) NADPH pools in cells depleted by 6-AN. (j) Elevated cystine levels in cells following 6-AN treatment. (k, l) WB of actin cytoskeleton protein in cells incubated 6-AN medium with or without TCEP in reducing and non-reducing conditions. (m) Fluorescence images of F-actin stained with rhodamine-phalloidin in cells cultured with or without 6-AN. Nuclei were stained by 4,6-diamidino-2-phenylindole (DAPI) (red: rhodamine-phalloidin; blue: DAPI) (TCEP = 2.5 mmol/L; Trion = 50 μmol/L; 6-AN, Fer-1, Z-VAD, Nec-1 = 20 μmol/L). Values are reported as means ± SD ($n = 3$). Scale bar: 5 μm. $^{*}P < 0.05$, $^{**}P < 0.01$, $^{***}P < 0.001$. ns, not significant.

cystine to cysteine by NADPH can elevate intracellular disulfides, we detected NADPH levels in SLC7A11^{high} OC cells following 6-AN treatment. The result displayed a significant decrease in NADPH levels (Fig. 1i). All these data indicated that 6-AN hinders the cystine breakdown by depleting NADPH, leading to a substantial accumulation of intracellular disulfide molecules, ultimately causing disulfidptosis in SLC7A11^{high} OC cells.

To validate our findings, we examined indicators related to disulfidptosis. ELISA assay was performed to measure intracellular cystine levels in SLC7A11^{high} OC cells with or without 6-AN. As depicted in Fig. 1j, the cystine concentrations were much higher in 6-AN-treated SLC7A11^{high} OC cells than that in the control group, indicating impaired cystine clearance. Concurrently, considerable disulfide bonds formation was observed in actin cytoskeletal protein, which could be effectively reduced by TCEP (Figs. 1k and l). Phalloidin can tightly and selectively bind to actin filaments (F-actin), stabilizing its structure. Therefore, phalloidin is extensively utilized for the qualitative and quantitative detection of F-actin [50]. So, we investigated the dynamics of actin cytoskeleton in SLC7A11^{high} cells cultured with 6-AN using rhodamine-phalloidin staining. Fluorescence confocal imaging revealed marked contraction and marginal clustering of F-actin in the presence of 6-AN treatment (Fig. 1m). Notably, the morphological changes of F-actin were consistent with the characteristics of disulfidptosis [19,22,51]. The result further highlighted the formation of numerous disulfide bonds in actin cytoskeletal protein. All these results demonstrated that 6-AN inhibits intracellular NADPH production, thereby disrupting cystine metabolism and causing the accumulation of disulfides, inducing disulfide stress. Eventually, this cascade of events triggers disulfidptosis in SLC7A11^{high} OC cells.

To enhance the therapeutic efficacy of 6-AN, we designed and synthesized the liposome system FA-L@AI. The construction of FA-L@AI is straightforward, and the specific synthesis method is detailed in methods (Scheme S1 in Supporting information). Transmission electron microscopy (TEM) images revealed that FA-L@AI forms spherical particles with an average diameter of approximately 100 nm (Fig. 2a and Fig. S4a in Supporting information). Dynamic light scattering (DLS) showed a hydrodynamic size of around 116 nm, with a polydispersion index (PDI) of about 0.21, indicating a uniform particle size distribution (Fig. 2b). Moreover, the hydrated particle size and PDI of FA-L@A and L@AI were comparable to those of FA-L@AI (Figs. S4b and c in Supporting information). Additionally, due to the negative charge imparted by FA modification on the surface, FA-L@AI exhibited a lower zeta poten-

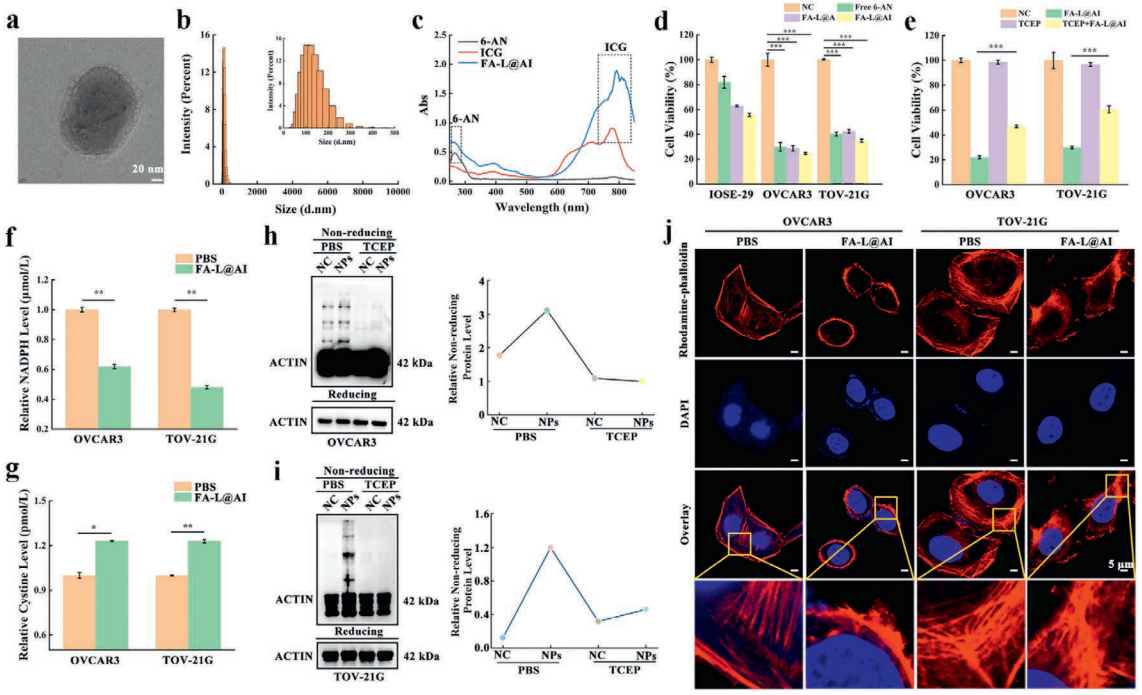


Fig. 2. The successful construction of FA-L@AI and its ability to mediate disulfidptosis in SLC7A11^{high} OC cells. (a) Larger-scale TEM image. Scale bar: 20 nm. (b) Hydrodynamic size of FA-L@AI. Insert, amplification area of the distribution. (c) Ultraviolet-visible spectroscopy (UV–vis) spectra of 6-AN (black line), ICG (red line) and FA-L@AI (blue line). (d) Cell viability of OC and normal cells treated with 26.74 μmol/L 6-AN (equal 0.2 mg/mL FA-L@AI), 0.2 mg/mL FA-L@A, 0.2 mg/mL FA-L@AI for 12 h. (e) Suppressing FA-L@AI-caused cell death by TCEP. (f) NADPH pools in cells depleted in the presence of FA-L@AI. (g) The nanodrug elevated cystine levels in cells. (h, i) Reducing and non-reducing WB of actin cytoskeleton protein in cells incubated with FA-L@AI medium containing or non-containing TCEP. NPs, FA-L@AI. (j) Fluorescence images of F-actin stained with rhodamine-phalloidin in cells cultured with or without FA-L@AI for 12 h. Nuclei were stained with DAPI (red: rhodamine-phalloidin; blue: DAPI) (FA-L@AI = 0.2 mg/mL, TCEP = 2.5 mmol/L). Values are reported as means ± SD ($n = 3$). Scale bar: 5 μm. $^{*}P < 0.05$, $^{**}P < 0.01$, $^{***}P < 0.001$.

tial value of −8.16 mV compared to −3.13 mV for L@AI (Fig. S4d in Supporting information). The detection of sulfur (S) in the elemental mapping further confirmed the valid incorporation of ICG into FA-L@AI (Fig. S4e in Supporting information). Meanwhile, the absorption spectra of FA-L@AI matched those of free 6-AN and free ICG, verifying the effective loading of both compounds (Fig. 2c). In brief, we successfully synthesized a nano-carrier system with a uniform size. According to Eqs. S1 and S2 (Supporting information) the encapsulation and loading efficiency of 6-AN were calculated to be 14 % and 2.3 %, respectively. While for ICG, these values reached 58 % and 9.7 %. Moreover, as shown in Fig. S5 (Supporting information), FA-L@AI possesses high optical and physical stability. In addition, the release of 6-AN and ICG were as high as 98 % and 78 % in lysosomal acidic environment, respectively (Fig. S6 in Supporting information). All these findings indicated that FA-L@AI is successful formulated and owns good stability.

We then assessed the ability of FA-L@AI to selectively accumulate in SLC7A11^{high} OC cells. OVCAR3 cells were stained with FA-L@AI for various durations, and the fluorescence intensities were recorded by flow cytometry. We observed a gradual increase in fluorescence intensity over time, with no significant changes noted after 1 h (Fig. S7 in Supporting information). Therefore, subsequent experiments were conducted with a standardized 1 h incubation period. Next, we evaluated the specificity of FA-L@AI towards cancer cells by culturing IOSE-29, OVCAR3, and TOV-21G cells with either FA-L@AI or L@AI. As shown in Fig. S8a (Supporting information), the red fluorescence (indicative of ICG) in IOSE-29, OVCAR3, and TOV-21G cells was surprisingly consistent when treated with L@AI. However, OVCAR3 and TOV-21G cells incubated with FA-L@AI exhibited stronger fluorescence compared to IOSE-29 cells. The fluorescence intensities in cancer cells were approximately three times higher than that in normal cells (Fig. S8b in Supporting information), indicating that FA-L@AI was more readily taken up by cancer cells due to the FA modification. Flow cytometry analysis further corroborated the imaging results (Fig. S9 in Supporting information). To further conform the high uptake of cancer cells to FA-L@AI by FRα mediated, we using additional FA treatment cells as a receptor-blocking model. In Fig. S10 (Supporting information), decreased signals were found in cells pretreated with FA, meaning an inhibited in uptake of nanodrugs. Furthermore, the colocalization coefficients of FA-L@AI and LysoTracker Red were 0.93 and 0.91, illustrating that FA-L@AI could enter in lysosomes through FRα-mediated endocytosis (Fig. S11 in Supporting information). In addition, FA-L@AI was distributed in cell membrane and lysosomes at 0.5 h, completely entering lysosomes at 1 h, subsequently releasing into cytosol at 1.5 h (Fig. S12 in Supporting information). According to Eq. S3 (Supporting information), the delivery efficiency of FA-L@AI to OVCAR3 and TOV-21G cells were calculated as 6.3 % and 4.9 %, respectively (Fig. S13 in Supporting information). These results affirmed the high accumulation of FA-L@AI in cancer cells, leveraging the overexpression of FRα.

Immediately, the cytotoxicity of FA-L@AI was measured by CCK-8 assay. The result indicated that the nanodrug has minimal effects on normal cells, but demonstrates substantial inhibition of SLC7A11^{high} OC cells at a dose of 0.2 mg/mL (Fig. S14 in Supporting information). Subsequently, cells were exposed to equally free 6-AN, FA-L@AI, and FA-L@A. All of these treatments significantly inhibited the activity of SLC7A11^{high} OC cells. Importantly, FA-L@AI and FA-L@A exhibited the same lethal effect as 6-AN, indicating that the FA-modified liposome carrier and ICG did not alter the toxicity of 6-AN (Fig. 2d). Additionally, FA-L@AI possessed the photothermal conversion properties under 808 nm light irradiation (Figs. S15 and S16 in Supporting information). All these data suggested that the nanodrug retains the efficacy of 6-AN and can specifically kill SLC7A11^{high} OC cells. Owing to its consistent

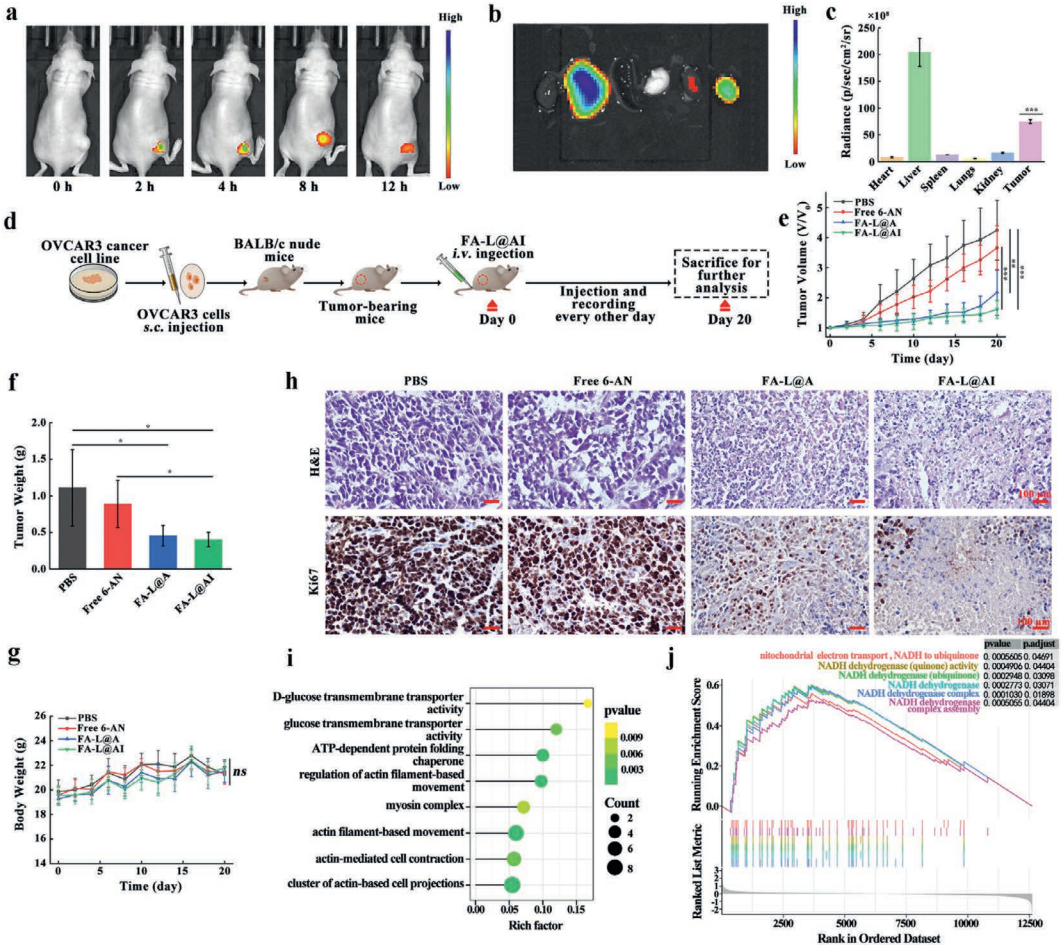


Fig. 3. FA-L@AI specifically trace OC tissues and exert antitumor effect. (a) *In vivo* images of tumor site in OC-bearing mice after FA-L@AI injected at different time. (b) Images of major organs (heart, liver, spleen, lung, and kidney) and tumor tissue removed from tumor-bearing mice after 12 h injection of FA-L@AI (2 mg/mL, 100 μL). (c) Quantitative analysis of major organs and tumors fluorescence intensities. Tumor compared to major organs. $^{***}P < 0.001$ by Student's *t*-test. (d) Schematic representation of the treatment regimen. (e) Tumor volumes were measured at various days post-injection with different drug treatments. (f) Weight of tumor masses after different treatments. $^{*}P < 0.05$. (g) Relative body weight changes during the treatment period. (h) H&E and Ki67 staining of tumor tissues after different treatments. (i) Gene ontology (GO) enrichment analysis of the differentially expressed genes (DEGs) between FA-L@AI and PBS groups. (j) Gene set enrichment analysis (GSEA) of NADH-related biological processes. Data are shown as mean ± SD ($n = 5$). Scale bar: 100 μm.

inhibitory effect comparable to free 6-AN, we hypothesized that the mechanism by which FA-L@AI induces harm to SLC7A11^{high} OC cells involves disulfidptosis. As depicted in Fig. 2e, the cell death caused by FA-L@AI was effectively reversed by TCEP, indicating the accumulation of disulfides in cells, much like the effect observed with free 6-AN. Furthermore, using an NADPH assay kit, we discovered that the NADPH levels in cancer cells treated with FA-L@AI were significantly lower compared to those in untreated cells (Fig. 2f). This finding clarified that FA-L@AI inhibits NADPH synthesis, thereby triggering disulfidptosis in SLC7A11^{high} OC cells.

These encouraging results prompt us to further evaluate the indicators related to disulfidptosis. The concentrations of cystine in cells treated with FA-L@AI dramatically elevated (Fig. 2g). Furthermore, WB analysis revealed that after treatment with FA-L@AI, there was a marked formation of disulfide bonds in actin cytoskeleton protein, which could also be suppressed by TCEP (Figs. 2h and i). Subsequently, SLC7A11^{high} OC cells were stained with rhodamine-phalloidin after a 12 h incubation with FA-L@AI. Fluorescence imaging showed notable contraction and marginal clustering of F-actin in cancer cells treated with the nanodrug, further corroborating the formation of disulfide bonds in actin cytoskeleton protein (Fig. 2j). Moreover, we also observed a notable morphological shrinkage of cells, which can be attributed to the disulfide bonds formation within F-actin. Collectively, these findings provided robust evidence that FA-L@AI preserves the lethal efficacy mediated by free 6-AN, which are characterized by the inhibition of NADPH synthesis, disruption of cystine metabolism, disulfides accumulation, and ultimately initiation of disulfidptosis.

All experiments involving mice were approved by the Animal Ethical Committee of Shandong University of Traditional Chinese Medicine (No. SDUTCM20240102001). To further assess the therapeutic potential of this nanodrug, we investigated the uptake capacity of the tumor for FA-L@AI in tumor-bearing mice models. Subcutaneous injection of OVCAR3 cancer cells into BALB/c nude mice to establish the tumor-bearing models. Following intravenous administration of FA-L@AI, *in vivo* images were captured. Notably, strong fluorescence was exclusively detected at the tumor site, peaking at 4 h post-administration and persisting for up to 12 h, indicating a prolonged residence time of FA-L@AI (Fig. 3a). Imaging of the major organs and tumor tissue revealed bright fluorescence in the tumor tissue, while normal tissues, except for the liver and kidney, exhibited dim fluorescence. This finding suggests a preferential accumulation of FA-L@AI in the tumor region, attributable to the EPR effect and the high expression of FRα on the cancer cell membrane (Fig. 3b). Furthermore, the fluorescence intensity in the tumor tissue was found to be 10 times greater than that in heart,

spleen and lungs (Fig. 3c). Meanwhile, bright fluorescence was also observed in the liver and kidney, primarily due to the influence of reticuloendothelial system [52–54]. Moreover, the fluorescence signal in mice after FA-L@AI injection was significantly stronger than that in L@AI treatment (Fig. S17 in Supporting information). Meanwhile, FA-L@AI has favorable biosafety and is excreted from mice within 36 h (Figs. S18 and S19 in Supporting information). Taken together, these results confirmed that FA-L@AI effectively aggregates and visualizes tumor locations based on FA-FA receptor affinity, providing the foundation for highly efficient therapy of OC.

Since FA-L@AI can highly accumulate in tumor tissue, whether it can exert a therapeutic effect on the tumor was explored. So we further tested the anti-OC effect of FA-L@AI in the tumor-bearing mice. The mice were randomly divided into four groups and received intravenous injections of the indicated drugs every other day. Tumor volumes were measured over a 20 day period to evaluate the therapeutic efficacy. The treatment scheme is shown in Fig. 3d. Compared to phosphate buffered saline (PBS) treatment, the size of tumors in the free 6-AN group showed a moderate reduction. In contrast, tumors in the FA-L@A and FA-L@AI groups exhibited significantly inhibition. Notably, the FA-L@AI injection displayed a remarkable growth inhibition compared to the free 6-AN group, suggesting that FA-L@AI exerts a potent antitumor effect without compromising its toxicity due to ICG loading (Fig. 3e). Researches indicate that FA can bind to FRα on tumor cells, and liposome can accumulate at tumor sites *via* EPR effect. Therefore, FA-L@AI achieved superior antitumor effects compared to the free drug. Furthermore, the trend in tumor weight was consistent with the volume measurements and tumor photograph (Fig. 3f and Fig. S20a in Supporting information). In addition, there was no significant changes in the weight of mice in FA-L@AI group, indicating that FA-L@AI has no systemic toxicity (Fig. 3g). In brief, we fully validated that our strategy utilizing FA-L@AI not only effectively improve the absorption of OC tissues, but also dramatically inhibits tumor growth through disulfidptosis.

To further demonstrate the antitumor efficacy of FA-L@AI *in vivo*, we conducted hematoxylin and eosin staining (H&E) and Ki67 staining on tumor tissues (Fig. 3h). Contrast with PBS group, no cell damage was observed in the free 6-AN group. However, tumor cells in the FA-L@A and FA-L@AI groups exhibited substantial cellular disruption, indicating the high therapeutic effect of FA-L@AI *in vivo*. What's more, the FA-L@A and FA-L@AI groups had the lowest Ki67 expression compared to other groups, suggesting its strong ability to inhibit tumor proliferation. All the results demonstrated the superior anti-tumor capability of FA-L@AI compared to free 6-AN. Additionally, we collected tumor tissues from the PBS and FA-L@AI groups for mRNA sequencing (Figs. S20b–d in Supporting information). Gene Ontology analyses revealed a striking enrichment of biological processes associated with actin cytoskeleton protein and glucose metabolism, implying that the nanodrug may cause intracellular alterations in actin cytoskeleton dynamics by affecting the glucose metabolism (Figs. 3i and j). These results further reinforced the notion that FA-L@AI triggers disulfidptosis in cancer cells, thereby effectively restraining tumor growth *in vivo*.

In this work, we identified significant over-expression of SLC7A11 in OC, and further demonstrated the glucose-dependent nature of SLC7A11^{high} OC cells. We elucidated that 6-AN-induced disulfidptosis effectively inhibits the growth of SLC7A11^{high} OC cells. To efficient delivery of 6-AN, a novel FA-modified liposomal nanodrug, FA-L@AI, was developed through a straightforward one-step self-assembly. The strategy fully preserved the efficacy of 6-AN and enhanced the tumor uptake. This is the first study that leverages disulfidptosis induced by 6-AN in SLC7A11^{high} OC cells to achieve the specific therapy of OC. FA-L@AI mainly exhibits three advantages: (1) Highly assimilated by OC cells with FA-modified; (2) specifically mediate disulfidptosis in SLC7A11^{high} OC cells, showing the forceful capability to erode these cells; and (3) selectively accumulated in tumor site and showed superior antitumor efficacy attributed to the FA modified and EPR effect, significantly inhibiting the growth of SLC7A11^{high} ovarian tumor with minimal systemic toxicity. Specifically, the involved therapeutic mechanism of disulfidptosis-triggered by FA-L@AI, which may offer an alternative to conventional therapies for OC treatment was further elucidated through mRNA transcriptome analysis. Generally, we design the pioneering nanodrug *via* a strategy by discerning the key gene, then exploring tumor cells specificity, and finally encapsulating the appropriate drug using a self-assembly method. We believe this study underscores a promising method for OC therapy, and contributes a robust evidence for advancing disulfidptosis-targeted approaches.

Declaration of competing interest

The authors declare that they have no known competing financial interests or personal relationships that could have appeared to influence the work reported in this paper.

CRediT authorship contribution statement

Nannan Fan: Writing – original draft, Project administration, Formal analysis, Data curation. **Zhen Zhang:** Funding acquisition, Formal analysis, Data curation. **Huiyan Zu:** Data curation. **Xinkui Liu:** Formal analysis, Data curation. **Bin Wang:** Data curation. **Xiuming Miao:** Data curation. **Chu Chu:** Data curation. **Yunhong Zhang:** Data curation. **Xiaoxiao Zhu:** Data curation. **Ping Li:** Writing – original draft, Validation, Supervision. **Xia Li:** Supervision, Project administration, Funding acquisition.

Acknowledgments

This study was supported by the National Natural Science Foundation of China (Nos. 82274575, 82474564, 82471704, 82405614), Major Basic Research Project of Shandong Natural Science Foundation (No. ZR2023ZD56), the Natural Science Foundation of Shandong Province (Nos. ZR2021MH175, ZR2022LZY011), Co-construction project of State Administration of TCM (Nos. GZY-KJS-SD-2023–034, GZY-KJS-SD-2023–046), Taishan Scholars Program (No. tstp20240513), Central Government Guides Local Science and Technology Development Fund Projects of Shandong Province (No. YDZX20203700001407). Key Laboratory of Traditional Chinese Medicine Classical Theory, Ministry of Education, Open Research Project. National Youth Qihuang Scholar Training Program and Shandong Province Traditional Chinese Medicine High Level Talent Cultivation Project. We special thank Professor Qiang Zou (Shanghai Institute of Immunology) for proving constructive suggestions.

Supplementary materials

Supplementary material associated with this article can be found, in the online version, at doi:10.1016/j.cclet.2025.111812.

References

[1] S. Lheureux, M. Braunstein, M. Amit, *CA* Cancer J. Clin. 69 (2019) 280–304.
[2] R.L. Siegel, K.D. Miller, N.S. Wagle, *CA* Cancer J. Clin. 73 (2023) 17–48.
[3] J.D. Seidman, S.I. Horkayne, M. Haiba, et al., Int. J. Gynecol. Pathol. 23 (2004) 41–44.
[4] D. Cortes-Guiral, M. Huebner, M. Alyami, et al., Nat. Rev. Dis. Primers 7 (2021) 91.
[5] C. Yang, B.R. Xia, Z.C. Zhang, et al., Front. Immunol. 11 (2020) 577869.
[6] L. Yu, Y.J. Xu, Z.J. Pu, et al., J. Am. Chem. Soc. 144 (2022) 11326–11337.
[7] Y.H. Fu, Y.C. He, X.D. Wei, et al., ACS Nano 18 (2024) 28793–28809.
[8] Y.X. Zhang, Q.Y. Jia, J. Li, et al., Adv. Mater. 35 (2023) 2305073.
[9] J.J. Cheng, L.L. Duo, D. Jin, et al., Angew. Chem. Int. Ed. 136 (2024) e202319982.

[10] X.L. Zhang, Y.X. Liu, H. Li, et al., Chin. Chem. Lett. 37 (2026) 111404.
[11] S.Q. Zhang, J.X. Li, X. Hu, et al., Chin. Chem. Lett. 36 (2025) 110314.
[12] X.Z. Wang, S.S. He, P.H. Cheng, K.Y. Pu, Adv. Mater. 35 (2023) 2206510.
[13] T.C. Do, J.W. Lau, C.X. Sun, et al., Sci. Adv. 8 (2022) 2216.
[14] C.S. Shin, P. Mishra, J.D. Watrous, et al., Nat. Commun. 8 (2017) 15074.
[15] P. Koppula, Y. Zhang, J.J. Shi, et al., J. Biol. Chem. 292 (2017) 14240–14249.
[16] T. Goji, K. Takahara, M. Negishi, H. Katoh, J. Biol. Chem. 292 (2017) 19721–19732.
[17] L.M. Machesky, Nat. Cell. Biol. 25 (2023) 375–376.
[18] X.G. Liu, L. Zhuang, B.Y. Gan, Trends. Cell Biol. 34 (2024) 327–337.
[19] X. Liu, L. Nie, Y. Zhang, et al., Nat. Cell Biol. 25 (2023) 404–414.
[20] W.Y. Zhen, Y.J. Fan, T. Germanas, et al., Adv. Mater. 37 (2025) 2405494.
[21] Y.L. Zhu, X.X. Wang, L.L. Feng, et al., Nat. Commun. 15 (2024) 8696.
[22] S. Guo, Z.H. Li, R.L. Zhou, et al., Small 20 (2024) 2309842.
[23] A. Mohanty, A. Mohapatra, W. Yang, et al., Adv. Healthc. Mater. 14 (2025) 2500272.
[24] W.Y. Zhen, T.Z. Zhao, X.Y. Chen, J.J. Zhang, Small 21 (2025) 2500880.
[25] X.D. Wu, S.Z. Shen, J.L. Qin, et al., BJOG 129 (2022) 40–49.
[26] I. Giacomini, E. Ragazzi, G. Pasut, M. Montopoli, Int. J. Mol. Sci. 21 (2020) 937.
[27] C.X. Wang, C.X. Yu, H.K. Chang, et al., Expert. Opin. Ther. Targt. 27 (2023) 733–743.
[28] Z. Song, S. Wang, L. Lu, et al., Metabolites 12 (2022) 1227.
[29] C.L. Song, Z.J. Jiao, Z.F. Hou, et al., J. Am. Chem. Soc. 145 (2023) 21860–21870.
[30] X.C. Fu, Y.M. Huang, H. Zhao, et al., Adv. Mater. 33 (2021) 2102570.
[31] X.Y. Li, H. Liu, W.Y. Gao, et al., Adv. Mater. 36 (2024) 2311291.
[32] X.Z. Lian, S. Chatterjee, Y.H. Sun, et al., Nat. Nanotechnol. 19 (2024) 1409–1417.
[33] M.M. Rahman, J. Wang, G.S. Wang, et al., Nat. Nanotechnol. 19 (2024) 818–824.
[34] W. Zhang, L. Ngo, S.C.H. Tsao, et al., ACS Appl. Mater. Interfaces 15 (2023) 16420–16433.
[35] J. Song, N. Zhang, L. Zhang, et al., Int. J. Nanomed. 14 (2019) 2757–2772.
[36] S.Y. Han, P. Dwivedi, F.A. Mangrio, et al., Artif. Cell Nanomed. B 47 (2019) 957–967.
[37] L.X. Li, D. He, Q.Q. Guo, J. Nanobiotechnol. 20 (2022) 50.
[38] C. Risnayanti, Y.S. Jang, J.J. Lee, H.J. Ahn, Sci. Rep. 8 (2018) 7498.
[39] L.Y. Jiang, H. Wang, S.Z. Chen, J. Nanosci. Nanotechnol. 20 (2020) 2025–2031.
[40] N.B. Mutlu-Agardan, C. Sarisozen, V.P. Torchilin, Pharm. Res. 37 (2020) 65.
[41] G.M. Dam, G. Themelis, L.M.A. Crane, et al., Nat. Med. 17 (2021) 1315–1319.
[42] G. Jo, B.Y. Lee, E.J. Kim, M.H. Park, H. Hyun, Biomedicines 8 (2020) 476.
[43] C. Ying, S.F. Wang, F. Zhang, Nat. Rev. Bioeng. 1 (2023) 60–78.
[44] W. Li, S.L. Yin, Y. Shen, L. Yuan, X.B. Zhang, J. Am. Chem. Soc. 145 (2023) 3736–3747.
[45] M. Zhang, W.T. Wang, M. Mohammadniaei, et al., Adv. Mater. 33 (2021) 2008802.
[46] W.Q. Meng, A.C. Sedgwick, N. Kwon, et al., J. Chem. Soc. Rev. 52 (2023) 601.
[47] X.L. Wang, B.B. Ding, W. Liu, et al., J. Am. Chem. Soc. 146 (2024) 17854–17865.
[48] M.S. Khan, B.H.J. Gowda, W.H. Almalki, et al., Drug Discov. Today 29 (2024) 103819.
[49] A. Gabizon, H. Shmeeda, A.T. Horowitz, S. Zalipsky, Adv. Drug Deliv. Rev. 56 (2004) 1177–1192.
[50] R.K. Hylton, J.E. Heebner, M.A. Grillo, M.T. Swulius, Nat. Commun. 13 (2022) 2439.
[51] M.J. Shi, X.Y. Li, Y. Guo, et al., Adv. Sci. 12 (2024) 2411131.
[52] M.S. Almeida, E. Susnik, B. Drasler, et al., Chem. Soc. Rev. 50 (2021) 5397.
[53] Z. Li, Y.B. Zhu, H.W. Zeng, et al., Nat. Commun. 14 (2023) 1437.
[54] A. Gabizon, A.T. Horowitz, D. Goren, et al., Clin. Cancer Res. 9 (2003) 6551–6559.